Depth dependent azimuthal anisotropy in the western US upper mantle

Huaiyu Yuan *, Barbara Romanowicz

Berkeley Seismological Laboratory, 215 McCone Hall, University of California-Berkeley, Berkeley, CA, USA, 94720

ABSTRACT

We present the results of a joint inversion of long period seismic waveforms and SKS splitting measurements for 3D lateral variations of anisotropy in the upper mantle beneath the western US, incorporating recent datasets generated by the USArray deployment as well as other permanent and temporary stations in the region. We find that shallow azimuthal anisotropy closely reflects plate motion generated shear in the asthenosphere in the shallow upper mantle (70–150 km depth), whereas at depths greater than 150 km, it is dominated by northward and upward flow associated with the extension of the East Pacific Rise under the continent, constrained to the east by the western edge of the North American craton, and to the north, by the presence of the East–West trending subduction zone. In particular, the depth-integrated effects of this anisotropy explain the apparent circular pattern of SKS splitting measurements observed in Nevada without the need to invoke any local anomalous structures.

© 2010 Elsevier B.V. All rights reserved.

1. Introduction

Various seismological approaches have been developed over the last 30 years to infer patterns of seismic anisotropy in the earth's mantle and provide constraints on past and present deformation processes. In particular, the analysis of SKS splitting measurements has been particularly useful for the study of upper mantle anisotropy (Fouch and Rondenay, 2006; Fouch et al., 2000; Levin et al., 1999; Savage, 1999; Silver, 1996; Silver and Chan, 1991; Vinnik et al., 1989). In the western US, such studies have revealed complex patterns of anisotropy (e.g., Currie et al., 2004; Davis, 2003; Fox and Sheehan, 2005; Gok et al., 2003; Hartog and Schwartz, 2000; Liu et al., 1994; Polet and Kanamori, 2002; Russo, 2009; Savage, 2002; Savage and Sheehan, 2000; Schutt et al., 1998; Waite et al., 2005; Walker et al., 2004; Wang et al., 2008; West et al., 2009; Xue and Allen, 2006), reflecting a strong correlation with the tectonic history of the region (e.g. Burchfiel et al., 1992), including subduction, passive rifting, transcurrent boundary deformation and intensive extension (Fig. 1).

The recent deployment of the Transportable Array (TA) of EarthScope, as well as several other temporary broadband networks in the western US, have provided the opportunity to measure SKS splitting at a significantly larger number of locations in the region than was previously possible. Combined with previously available SKS splitting data, these measurements have revealed an intriguing apparent "circular" pattern in the distribution of fast axis directions

and amplitude of anisotropy, centered in south-central Nevada, with vanishing strength in the center of the pattern (Eakin et al., 2010; Liu, 2009; Savage and Sheehan, 2000; Schutt and Humphreys, 2001; West et al., 2009). In addition to the circular SKS splitting pattern, large splitting times (~2 s) are observed beneath Oregon and western Idaho (Long et al., 2009; Xue and Allen, 2006), much larger than the 1 s global continent average (Silver, 1996). Interestingly, some recent regional body wave tomographic studies also show the presence of a fast velocity anomaly extending into the transition zone, beneath the Cascades and High Lava Plains (e.g., Burdick et al., 2009; Sigloch et al., 2008; van der Lee and Nolet, 1997; Xue and Allen, 2007). Various geodynamic models have been proposed to address the mantle flow associated with these features, including: 1) initial impinging of an active upwelling into the lithosphere in the Basin and Range province (Savage and Sheehan, 2000; Walker et al., 2004); 2) toroidal flow around the southern edge of the sinking Gorda–Juan de Fuca plate, associated with its retreating and the creation of a slab window (Zandt and Humphreys, 2008); and 3) asthenospheric flow associated with a sinking lithospheric instability (or "drip") in the center of the Basin and Range (West et al., 2009).

While providing improved lateral resolution, the SKS dataset by itself lacks the depth resolution necessary to constrain the 3D pattern of anisotropy in the upper mantle, even though the necessity of introducing several layers of anisotropy in the upper mantle to explain SKS splitting data has been demonstrated (e.g., Levin et al., 1999; Özalaybey and Savage, 1994; Silver and Savage, 1994; Yuan et al., 2008). Therefore, we have performed a combined inversion of long period fundamental mode and overtone surface waveforms and SKS splitting data for anisotropic shear velocity structure in the upper

* Corresponding author. Tel.: +1 510 6428374.
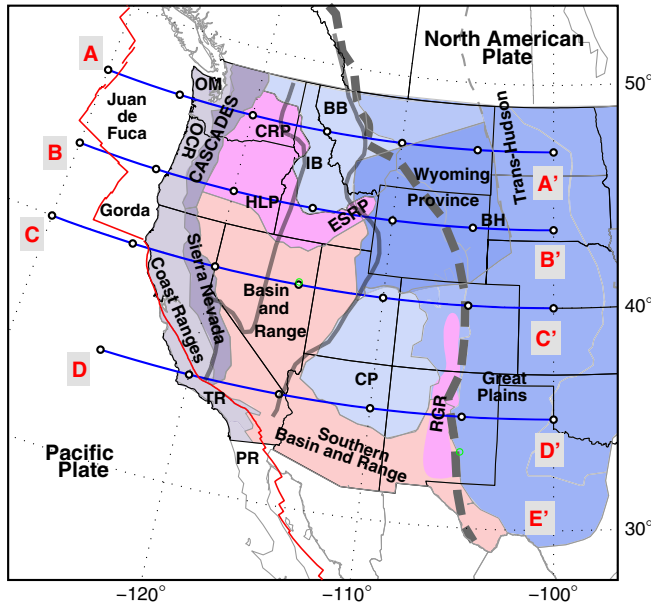 *E-mail address:* huaiyu.yuan@berkeley.edu (H. Yuan).

Fig. 1. Tectonic setting and physiographic provinces of the western US. Labels follow Burchfiel et al. (1992): OM, Olympic Mountains; OCT, Oregon Coast Ranges; CRP, Columbia River Plateau; BB, Belt Basin; IB, Idaho Batholith; HLP, High Lava Plains; ESRP, Eastern Snake River Plain, BH, Black Hills; CP, Colorado Plateau; RGR Rio Grande Rift; TR, Transverse Ranges; and PR, Peninsular Ranges. Red line demarcates the boundary between the Pacific Plate and the North American (NA), Gorda and Juan de Fuca plates. The thick gray dashed line is the Rocky Mountain Front. The two thin gray lines are the Sevier Thrust and Fold belt, and the Strontium isotope ratio 0.706 line, which, respectively, mark the eastern and western boundaries of the Precambrian passive margin of the continent (Burchfiel et al., 1992). The locations of depth cross-sections AA′ to DD′ discussed in the text are shown as blue lines.

mantle over the North American continent. Our complete model (Yuan and Romanowicz, 2010; Yuan et al., in revision) includes 3D isotropic shear velocity (*Vs*) structure, radial anisotropy, described by the parameter $\xi = (V_{sh}/V_{sv})^2$, and azimuthal anisotropy. We focus here specifically on the 3D distribution of azimuthal anisotropy and on the tectonic provinces west of the Rocky Mountain Front, where the USArray Transportable Array (TA) provides the most dense station coverage for both surface waveform and SKS measurements in the whole continent. In particular, we show that the apparent circular pattern in SKS splitting in Nevada can be explained simply by a depth dependent anisotropic structure in the upper mantle, expressing the rapid transition from shear dominated by the North American plate motion (NA) in the east, to shear dominated by Pacific plate motion (PAC) in the west, in the presence of the sinking Juan de Fuca plate in the north, and the northward extension of the East Pacific Rise (EPR) in the south.

2. Azimuthal anisotropic tomographic inversion

Our inversion follows the methodology described in Marone and Romanowicz (2007) and Marone et al. (2007) (from here on referred to as MR07). As in MR07, the tomographic waveform inversion is cast in the framework of non-linear asymptotic normal mode coupling theory (NACT, Li and Romanowicz, 1995) which takes into account coupling across mode branches, thus allowing us to represent the body wave character of overtones by means of 2D finite frequency kernels in the vertical plane containing source and receiver. In what follows, we describe the dataset used, the model parameterization and the key steps of our inversion procedure. More details on our azimuthal anisotropy tomography method are found in our companion papers (Yuan and Romanowicz, 2010; Yuan et al., in revision).

2.1. Joint inversion with SKS splitting measurements

Assuming weak anisotropy with a horizontal fast symmetry axis and long enough period of the SKS waves (i.e., >10 s), we can express the station-averaged SKS splitting measurements (apparent splitting time δt and fast axis direction ψ) as a function of elastic parameters as (e.g., Marone and Romanowicz, 2007; Montagner et al., 2000):

$$\delta t \sin 2\psi = \int_0^a \frac{1}{V_s^0(z)L^0(z)} G_s(\theta, \varphi, z) dz \tag{1}$$

$$\delta t \cos 2\psi = \int_0^a \frac{1}{V_s^0(z)L^0(z)} G_c(\theta, \varphi, z) dz \tag{2}$$

where a is the Earth radius, and θ, φ, z describe the position in the spherical Earth. $L = \rho V_{SV}^2$, where ρ is density, is one of the five Love parameters (A, C, F, L, and N; Love, 1927). $V_S = \sqrt{(2L + N)/(3\rho)}$ is isotropic S-velocity. The two azimuthal anisotropy terms, $G_s = G\sin(2\psi_G)$ and $G_c = G\cos(2\psi_G)$, depend on the local anisotropy strength G and fast axis direction ψ_G at a point (θ, φ, z) with $G = \sqrt{G_s^2 + G_c^2}$ and $\psi_G = \frac{1}{2} \arctan\left(G_s / G_c\right)$ (Montagner and Nataf, 1986; Montagner et al., 2000). We substitute L in the original derivation (Montagner et al., 2000) with L^0 assuming weak anisotropy. Superscript 0 refers to the parameters of the one-dimensional reference model.

Eqs. (1) and (2) set up an inversion problem for the two azimuthal anisotropy parameters G_s and G_c using the SKS splitting data (δt and ψ). Parameters G_s and G_c can also be retrieved from surface waveform inversion (e.g. Marone and Romanowicz, 2007; Yuan et al., in revision). Eqs. (1) and (2) and the fact that the waveforms and SKS splitting data are sensitive to the same parameters G_c and G_s allow us to combine the two datasets and set up a joint inversion for G_s and G_c.

Eqs. (1) and (2) can be rearranged as

$$\delta t = \sqrt{\left(\int_0^a \frac{1}{V_s^0(z)L^0(z)} G_s(\theta, \varphi, z) dz\right)^2 + \left(\int_0^a \frac{1}{V_s^0(z)L^0(z)} G_c(\theta, \varphi, z) dz\right)^2} \tag{3}$$

$$\tan 2\psi = \frac{\int_0^a \frac{1}{V_s^0(z)L^0(z)} G_s(\theta, \varphi, z) dz}{\int_0^a \frac{1}{V_s^0(z)L^0(z)} G_c(\theta, \varphi, z) dz} \tag{4}$$

Using Eqs. (3) and (4) the predicted SKS splitting parameters, δt and ψ can be computed by integrating the inverted G_s and G_c over depth (V_s^0 and L^0 are known from the 1D reference model).

To be valid, the formalism of Montagner et al. (2000) requires that the dominant period of SKS measurements be greater than ~10 s, which is in general the case in studies that contribute to our SKS compilation. As a first order approximation, the formalism here does not include finite frequency effects on the SKS measurements (e.g., Favier and Chevrot, 2003; Rümpker et al., 1999; Sieminski et al., 2008). Long and Silver (2009) discuss the frequency dependence of splitting measurements in the presence of multiple layers of anisotropy, and point out that higher frequency measurements are generally biased towards near surface layers. Inspecting finite frequency kernel effects for the SKS measurements may become useful when moving to higher resolution in our inversion.

δt and ψ given by Eqs. (3) and (4) predict apparent splitting parameters, which represent the integrated effects of shear wave splitting through a depth dependent (e.g., multiple-layer) anisotropic domain. Our dataset of station-averaged SKS is a compilation from recent studies by several groups (Courtier et al., 2010; Eakin et al., 2010; Frederiksen et al., 2006; Liu, 2009; West et al., 2009) thus we do not possess details of how the station averages were performed. In

general, such stations averages are obtained using an error surface stacking method (e.g., Wolfe and Silver, 1998; Yuan et al., 2008) from individual events which should include measurements over a wide range of back-azimuths, so that the station averages are good representations of the apparent splitting at the earth's surface.

Strong back-azimuth dependence is reported from individual SKS measurements in the western US (e.g., Liu et al., 1994; Özalaybey and Savage, 1995; Polet and Kanamori, 2002), suggesting the existence of multiple layers or dipping anisotropy. Our inversion method could be modified to incorporate Individual measurements. We consider station-averaged rather than individual SKS measurements, however, to avoid contamination by the possible presence of anisotropy outside of our model space (e.g. the core–mantle boundary region; Long, 2009): by station averaging, the incoherent signal along the ray path outside of our model region is effectively muted, while consistent anisotropic signals from the single- or multiple-layered upper mantle structure within our model space contribute to the apparent splitting measurements on the surface.

2.2. Data and inversion procedure

We complemented the three-component teleseismic waveform data collection of MR07 with recent data from permanent and temporary broadband stations in North America, in order to achieve higher spatial resolution and improved azimuthal distribution. In particular, owing to the uniform coverage provided by the 70-km spacing TA stations, and earthquakes from three regions (the Aleutians and the western Pacific, Tonga, and South America) with abundant seismicity, we obtain excellent azimuthal coverage for the western US (Fig. 2). Our waveform dataset now includes over 150,000 fundamental and overtone wave packets, in which three-component seismograms from ~1100 Mw 6 to 7 teleseismic events recorded at over 1500 stations are decomposed into individual energy packets, which can be separately weighted in the inversion to bring out the contribution of smaller amplitude phases (e.g., fundamental versus overtone surface waves; Li and Romanowicz, 1995; Panning and Romanowicz, 2006). The SKS splitting data collection of MR07 was also complemented by more recent measurements from the literature (Eakin et al., 2010; Liu, 2009; West et al., 2009) resulting in a total of more than 1200 station-averaged SKS measurements.

The waveform data were low pass filtered with a cut-off period of 60 s, and corrected for the influence of structure o`utside of the region

of study using a recent 3D radially isotropic global shear velocity model of the upper mantle developed with the Spectral Element Method (SEMum; Lekic and Romanowicz, 2010). Crustal corrections were applied using the CRUST2.0 model (Bassin et al., 2000) and an approach that takes into account the non-linearity introduced by large variations in Moho depth (Lekic and Romanowicz, 2010).

The inversion then proceeded in two steps. The waveform data were first inverted for 3D Vs and ξ structure in the upper mantle, down to 1000 km, under the entire North American continent. In a second step, the waveform dataset, corrected for the 3D Vs and ξ structure obtained in the first step, was jointly inverted with station-averaged SKS splitting data for 3D variations in 2-ψ azimuthal anisotropy, using the formalism of Montagner et al. (2000) described above. G_s and G_c are the only azimuthal anisotropy parameters (Montagner and Nataf, 1986) that can be resolved well using long period waveforms, given the available azimuthal distribution of data. A relative weight is needed to take into account the scaling between the two types of data. As shown in our previous and companion papers (Marone and Romanowicz, 2007; Yuan and Romanowicz, 2010; Yuan et al., in revision), models obtained by adding the SKS splitting data do not significantly change the fit to the waveforms. Thus the optimum weight is found by picking the elbow value of the variance reduction versus model norm trade-off curve for the SKS data (e.g. Supp. Fig. 4 in Yuan and Romanowicz, 2010). As shown in the next section, addition of SKS splitting constraints improves depth resolution of azimuthal anisotropy at depths greater than 250 km, without degrading the fit to the waveform data.

3. Azimuthal anisotropy inversion results

The continental scale azimuthal anisotropy model obtained is described elsewhere (Yuan and Romanowicz, 2010; Yuan et al., in revision). In what follows, we discuss the azimuthal anisotropy results in the western part of the continent. We limit our discussion to the first 500 km of the upper mantle, where our model is best resolved in depth. Indeed, at depths from 24 km to 500 km, we are able to parameterize the model in depth using cubic splines with spacing 30–70 km (Fig. 3a), while the spline spacing changes to 150 km and greater at larger depths, based on resolution tests. The lateral parameterization of the model is in terms of an unconformal spherical spline mesh (Wang and Dahlen, 1995) with a mesh for Vs corresponding to lateral resolution of about 250 km and a mesh for
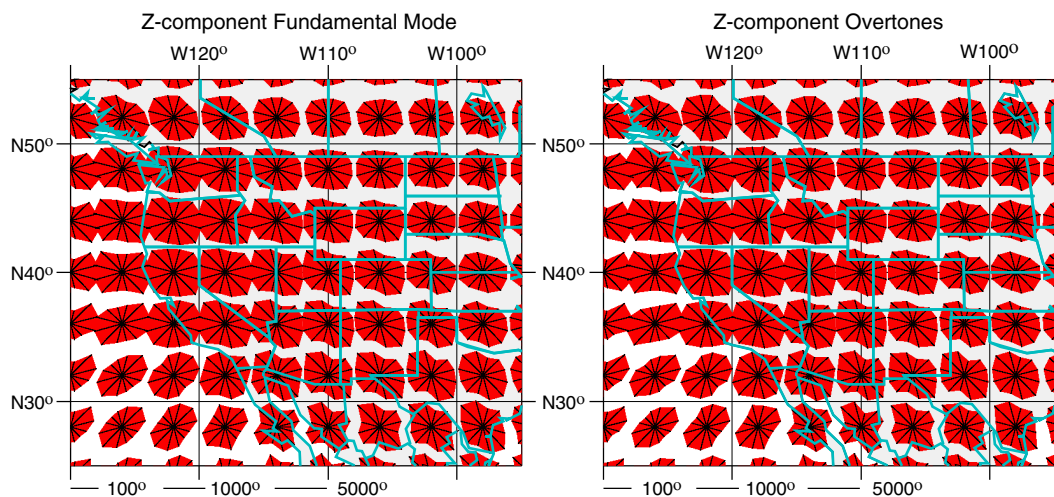

Fig. 2. Azimuthal coverage provided by minor arc source-station paths for fundamental (left) and high mode (right) waveforms for the vertical component. Blue bars plotted at the center of each 4° by 4° region show the cumulative source-station paths within 30° azimuthal bins. The scale is logarithmic. Note in majority of the nodes the wide azimuthal coverage provided by the events from the Aleutians and the western Pacific, Tonga and South America.
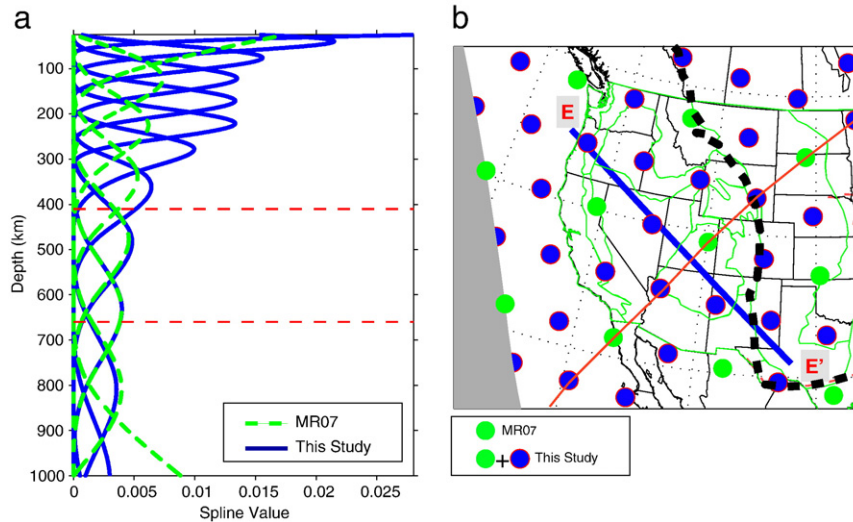
Fig. 3. Model parameterization for our inversion. (a) Vertical cubic splines used in this study (blue) and in MR07 (dashed green). Note the finer spatial resolution in our inversions allowed by the inclusion of the TA data. (b) "Level 5" spherical spline nodes (green and blue dots) with 4° spacing, corresponding to the resolution of a degree 48 spherical harmonics model. "Level 4" nodes (corresponding to 8° spacing and a degree 24 spherical harmonics model) used in MR07 are shown as green dots only for comparison. Blue line is the location of depth profile EE′ for the resolution test in Figure 4. Red line is the vertical symmetry plane for forming the input model in our resolution test (see details in text).

radial and azimuthal anisotropy corresponding to lateral resolution of about 450 km (Fig. 3b). The parameters are parameterized vertically in terms of B-splines (Fig. 3a; Mégnin and Romanowicz, 2000).

3.1. Resolution

A series of resolution tests are presented in the companion papers to show the robustness of our joint tomographic inversions for the 3-D North American upper mantle isotropic and anisotropic structure. Checkerboard-like structure (e.g. in Yuan and Romanowicz, 2010) and more realistic synthetic models, which are taken and modified from our inverted models and therefore have broader spectrum of velocity heterogeneities (e.g. Nettles and Dziewoński, 2008), are tested using the model resolution matrix (Menke, 1989). The recovered models are suitable to address the resolution power of the current dataset and the effects of the applied damping scheme (e.g. Marone et al., 2007). Specifically for the azimuthal anisotropy inversion, our tests show that, 1) we are able to accurately recover the distribution of fast axis directions of azimuthal anisotropy down to the transition zone; 2) the azimuthal anisotropy strength is systematically underestimated at larger depths (>200 km), particularly so when inverting waveforms only; 3) the recovery of azimuthal anisotropy amplitude at depths larger than 200 km is improved by the addition of constraints from the SKS dataset (Marone et al., 2007; Yuan and Romanowicz, 2010; Yuan et al., in revision).

In Figure 4 we show an example of a resolution test along a depth cross-section EE′, which runs diagonally through our western US model region. The input model is modified from our inverted model using both the waveform and SKS data sets. To form the input model, the inverted model is spatially flipped by symmetry with respect to a vertical plane to avoid possible bias introduced by the current data distribution (see also Supp. Figs. 8 and 9 in Yuan and Romanowicz (2010)). The recovered models, particularly for the inversion which includes the SKS dataset, can accurately recover the 3D distribution of fast axis directions of azimuthal anisotropy down to the transition zone. Figure 4 also shows that the inversions with and without the SKS dataset (middle and bottom panels in Fig. 4) yield similar anisotropic structures in the upper 200 km for both amplitude and fast axis direction distribution. Below 200 km, anisotropy strength is better recovered from the inversion that includes the SKS dataset, while the directions do not change much whether or not the SKS

dataset is included. The stability of the direction recovered below 200 km suggests that the two datasets are compatible, as also found at the global scale (Wüstefeld et al., 2009), and that the enhanced anisotropy strength below 200 km (middle right panel in Fig. 4) when SKS data are included is not an artifact.

3.2. Azimuthal anisotropy patterns in the Western US upper mantle

Figure 5 shows maps of lateral variations in azimuthal anisotropy at different depths in the upper mantle. In Figure 6, we present several East–West depth cross-sections in Vs and azimuthal anisotropy across the region of study. Several spatial domains can be distinguished. First, the Rocky Mountain Front (RMF) marks a sharp boundary between, to the east, the North American craton with thick lithosphere (200–250 km), and, to the west, a domain with thin lithosphere (50–80 km), as determined from receiver function studies (Abt et al., 2010; Li et al., 2007) as well as from our isotropic Vs and ξ inversion (Yuan et al., in revision). Under the craton, weak azimuthal anisotropy is present in the lithosphere, markedly changing in direction and strength at the lithosphere–asthenosphere boundary (LAB) (Yuan and Romanowicz, 2010). Azimuthal anisotropy is stronger at depths greater than 200 km, peaking around 250 km (e.g., Fig. 4) with a NE–SW fast axis direction parallel to the North American absolute plate motion (NA APM; Gripp and Gordon, 2002). Patterns of anisotropy in the NA craton upper mantle are described in more detail in Yuan and Romanowicz (2010), and we will not discuss them further here.

West of the RMF, results are shown at and below 70 km, and correspond to asthenospheric depths. Several domains can be distinguished. At the southwest corner of the region considered, under the Pacific Plate and west of the San Andreas Fault, the fast axis direction is parallel to the Pacific Plate APM throughout the depth domain considered, and the strength of anisotropy peaks in the depth range of 150–200 km. In the region between the craton and the Pacific ocean, and from north to south, anisotropy is strong at shallow depths (70–100 km), with a NE–SW pointing fast axis direction, quasi parallel to both the NA and Juan de Fuca/Gorda plate APM, and decreases with depth, reaching a minimum around 150 km depth. It appears that, at shallow depth in the western US, the azimuthal anisotropy pattern reveals strong shear associated with coupling between the asthenosphere and lithosphere in the NA and Juan de Fuca (JdF) plates on the
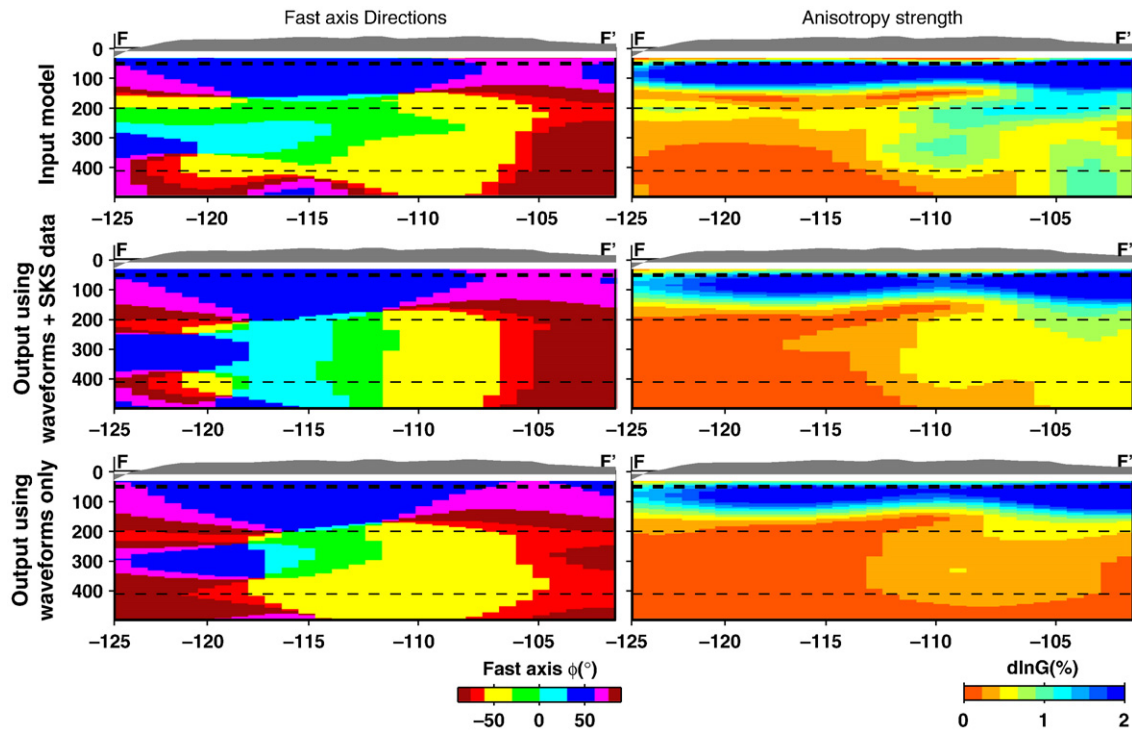
Fig. 4. Resolution test for azimuthal anisotropy direction and strength along depth profile EE′, which runs diagonally across our model region (Fig. 3). We consider as input model, the 3D azimuthal anisotropy model obtained from our joint inversion, and modified by flipping its lateral structure with respect to a vertical symmetry plane (indicated by the red line in Fig. 3) to avoid possible bias introduced by current data distribution. The output models are obtained by multiplying the input model by the respective resolution matrices corresponding to joint inversion with SKS splitting data and inversion using waveforms only. *Top panels*: Input distribution of fast axis direction (left) and strength (right). *Middle panels*: Recovered fast axis direction (left) and strength (right) from the model obtained from joint inversion of waveforms and SKS splitting data. *Bottom panels*: recovered fast axis direction (left) and strength (right) for the model obtained using waveform data only. In the left panels, the color indicates direction of the fast axis. The fast axis direction of the input model is well recovered in both models, whereas the strength of anisotropy is poorly recovered below 200 km when only waveforms are inverted, as we have previously observed (e.g. Marone and Romanowicz, 2007; Yuan and Romanowicz, 2010). At depths greater than 500 km (not shown), depth resolution is poor in all cases, resulting in smearing of features with depth.

eastern side, and in the PAC plate on the western side of the PAC/NA/JdF plate boundaries. The 150 km depth marks a large scale transition in the anisotropy direction. At this depth under Oregon, Nevada, and much of California, the fast axis direction takes on an intermediate East–West direction between the NA and PAC APMs, as seen in many other studies (e.g., Becker et al., 2006; Beghein et al., 2010; Lin et al.,
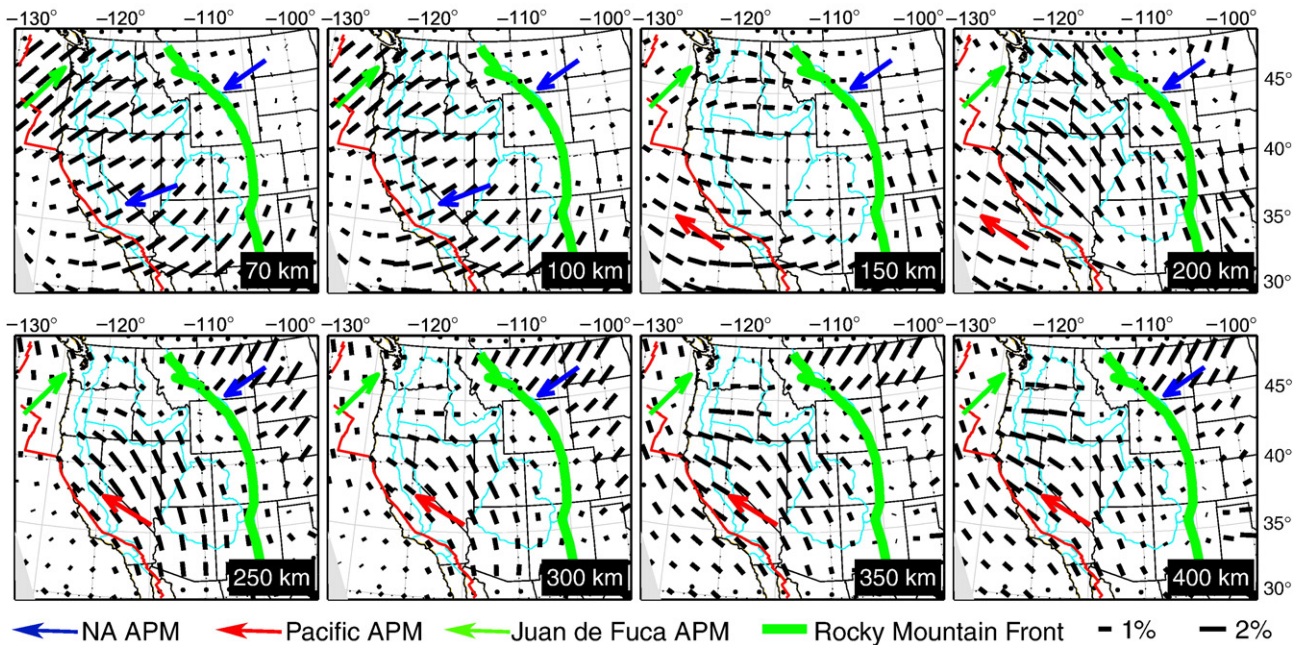

Fig. 5. Azimuthal anisotropy variations with depth. Black bars indicate the fast axis direction and the bar length is proportional to the anisotropy strength. Blue, green and red arrows show the absolute plate motion (APM) directions of the North American, JdF, and the Pacific plates, respectively, computed at each location using the HS3-NUVEL 1A model (Gripp and Gordon, 2002). Thick green line is the Rocky Mountain Front. Physiographic provinces are outlined in cyan as in Fig. 1.
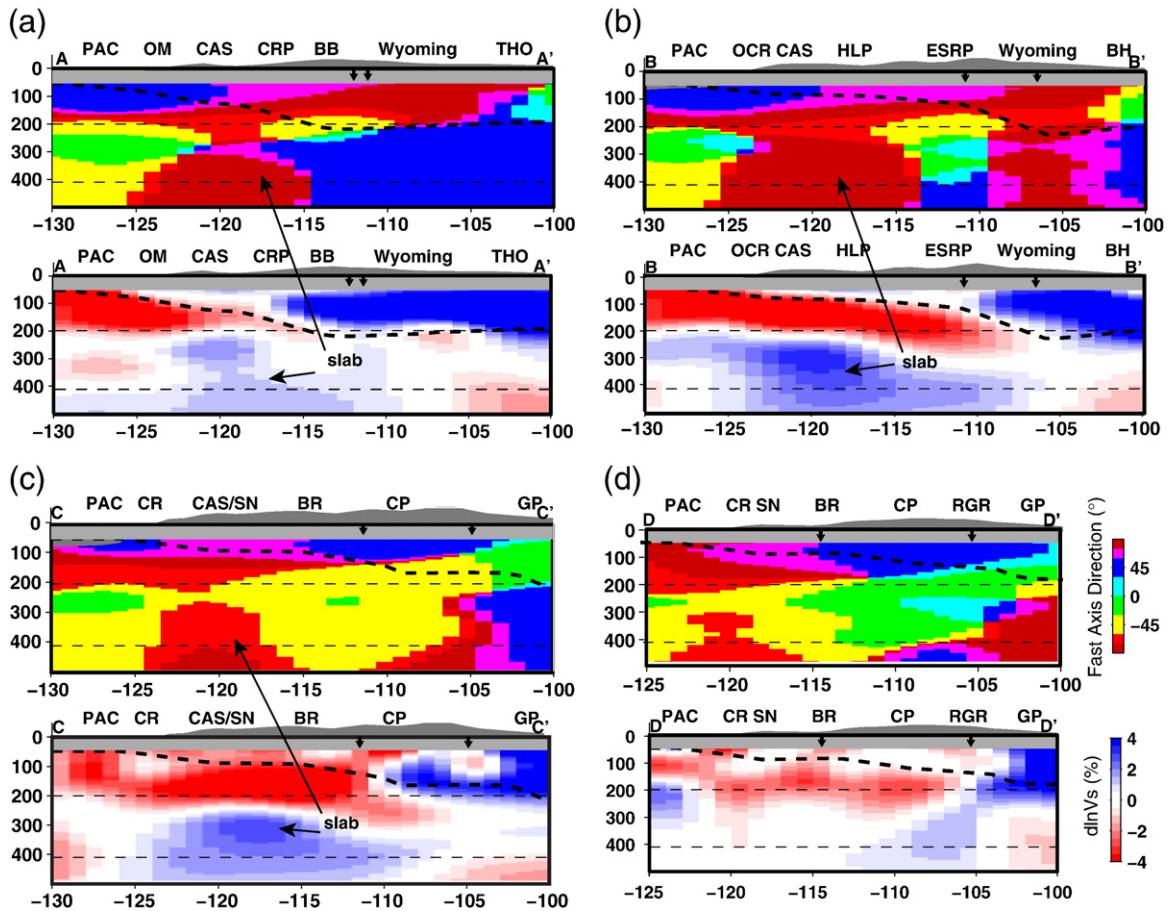
Fig. 6. Depth cross-sections of azimuthal anisotropy compared with variations in *Vs* along East–West cross-sections shown in Figure 1: (a) AA′, (b) BB′, (c) CC′, (d) DD′. For each cross-section, the top and bottom panels show the azimuthal anisotropy and isotropic velocity, respectively, with each their own color scale, as given (d). For anisotropy, the color indicates the direction of the fast axis. The LAB estimated from the location of the maximum gradient with depth of *Vs* and ξ is shown as the thick dashed black line. Note that due to the 180° ambiguity, the east and west pointing fast axis directions are equivalent (dark red). Physiographic provinces are indicated at the top of each cross section following Figure 1. The two arrows indicate the location of the Sevier Fold and Thrust belt (left) and Rocky Mountain Front (Right), respectively. We present results for depths greater than 50 km as resolution is poor at shallow depths. In (a) (b) and (c), the coincident location of fast velocities and East–West trending anisotropy are marked as "slab". Cross section DD′ (d) is south of the termination of the fast velocity feature in the transition zone. In DD′, the East–West trending anisotropy region is very narrow, indicating that the influence of the slab-like feature extends south beyond its termination. The fast velocity region seen further east in the *Vs* cross-section is found in many tomographic models and is attributed to the lost Farallon slab. It is not directly connected to the feature seen at similar depths in (a) (b) (c).

2009; Silver and Holt, 2002; Yang and Forsyth, 2006; Zhang et al., 2009).

Below 150 km, the anisotropy becomes stronger again, first under Oregon and Washington (200 km) and somewhat deeper under the Basin and Range (250 km), and the fast axis has rotated to a direction quasi parallel to the Pacific Plate APM, almost orthogonal to the NA APM. A region of N–S oriented fast axis appears at 250 km depth under the Colorado Plateau and southern Basin and Range, peaking in strength between 250 and 350 km, while an East–West oriented domain begins at 250 km depth under Oregon and Washington states, peaking in strength at 400 km. This region coincides laterally and in depth with the location of a fast *Vs* anomaly that has been associated with the presence of the subducted Juan de Fuca plate (e.g., Xue and Allen, 2007). Indeed, as revealed by our isotropic velocity model (Fig. 6a–c and Yuan et al., in revision) and many other tomographic studies, high velocities are found beneath the Cascades and the High Lava Plains at depths below 200 km, and extend to transition zone depths beneath the Basin and Range. The on-going Juan de Fuca subduction and the subducted Farallon slab are likely responsible for the high velocity anomalies. While our lateral resolution is insufficient to detect the thin slab at depths shallower than 200 km, the slab is quite visible both in velocity and in anisotropy at transition zone depths and just above, where it has spread laterally. The coincidence between the E–W pointing anisotropy domain and the fast

velocities down to transition zone depths is particularly clear when comparing depth cross-sections of *Vs* and azimuthal anisotropy along East–West profiles, as shown in Figure 6a–c. The fast axis direction remains East–West beneath the northern Cascades and the Columbia River Plateau, and rotates slightly to WNW in the High Lava Plains and the northwestern Basin and Range. Neither East–West nor WNW direction correlates with the NA JdF and Gorda APM or the predicted NW–SW Pacific APM (Gripp and Gordon, 2002). We note that the trend of the Cascades in Oregon, where the JdF slab steepens dramatically (McCrory et al., 2006; Xue and Allen, 2010), has a general North–South direction. We suspect that the high velocity body in the transition zone is related to the stagnant subducted JdF slab, while the East–West fast axis direction associated with the high velocities may be due to flow around the southern edge of the slab, as well as internal deformation within the stacked slab segments (e.g., Schmid et al., 2002).

Also starting at a depth of ~200 km, a narrower anisotropic domain with North–South to NNW–SSE fast axis direction is present between the subduction system and the craton. As can be seen from depth cross-sections shown in Figure 6, this N–S oriented fast axis domain extends horizontally from the southern Basin and Range and the Rio Grande rift system (−115° and −105° on DD′) to beneath the western edge of the Wyoming province (−115° to −110° on BB′), and is associated with the broad low *Vs* region marking the northern

continuation of the East Pacific Rise, as seen in both regional and global shear velocity models (e.g., Kustowski et al., 2008; Nettles and Dziewoński, 2008; Panning and Romanowicz, 2006), as well as a region of radial anisotropy with ξ<1 (Yuan et al., in revision), indicative of the presence of a vertical component of shear. This northerly pointing direction rotates more to NW–SE along the Sevier Thrust and Fold belt beneath the northeastern Basin and Range, following the shape of the western edge of the North American craton, and rotates to East–West beneath the Snake River Plain and the High Lava plains, as described above. We suggest that the overall pattern of anisotropy at depths greater than 150 km is controlled by flow moving northward and up from the East Pacific Rise (EPR), guided by the southwestern border of the craton, in the southern US and by the presence of the slab stagnating in the transition zone in the northwestern US as mentioned above. Several large scale azimuthal anisotropy studies observe this generally North–South to NNW–SSE direction fast axis at 200 km in the region (Maggi et al., 2006; Montagner, 2002; Smith et al., 2004). Interestingly, this is also in agreement with the northward component of the deep flow from independent geodynamic modeling based on isotropic tomographic models (e.g., Forte et al., 2010).

4. Depth dependent SKS splitting: the circular pattern and large splitting times

As described above, we find a strongly depth dependent azimuthal anisotropy pattern in the western US, with orientation of the fast axis

controlled by plate motion related lithosphere–asthenosphere coupling at depths shallower than 150 km, and other processes at greater depths, likely representing the channeling of deep flow from the EPR constrained by the presence of the craton margin to the west and subducted slabs to the north. We infer that all these features combined significantly contribute to the circular pattern and large splitting times of the SKS splitting observations.

Indeed, the SKS splitting predictions from our inverted model successfully predict the circular splitting measurement pattern (Fig. 7a). Integrating different depth portions of our model shows that the circular pattern is best reproduced by integrating the azimuthal anisotropy model over the full upper mantle depth range. In Figure 7b, we plot the SKS predictions from the top 150 km of our model. The predicted splitting directions are to first order parallel to the NA APM in most of the western US and to the PAC APM offshore. It is thus clear that this shallow depth anisotropy domain contributes to the NA APM parallel (NE–SW) component of the surface SKS circular pattern. This portion of the model provides about 34% variance reduction. The deeper anisotropy domain (150–500 km, Fig. 7c) contributes a significant northward apparent splitting direction in the southern Basin and Range and along the Colorado Plateau. Under southern and central California, the predicted apparent splitting has a NW–SE direction, perpendicular to that seen at shallow depth, and close to the Pacific Plate APM. The NW–SE direction beneath the northeastern Basin and Range and southern and central California thus contributes to the NW–SE component of the circular pattern seen in the SKS splitting. Variance reduction from the deeper portion of the
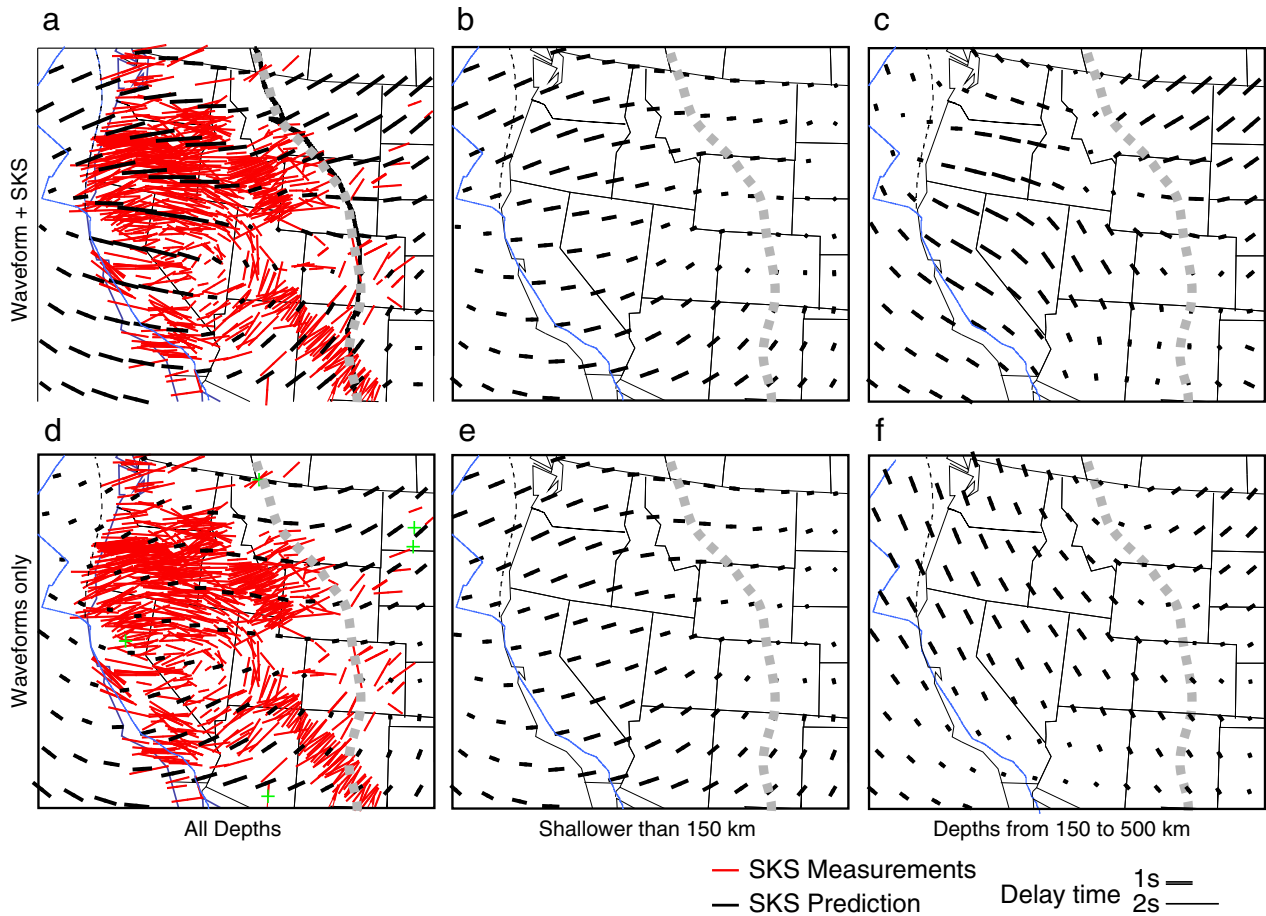

Fig. 7. Comparison of observed and predicted apparent splitting parameters. Red bars indicate observed station-averaged SKS splitting measurements and are shown in the left panels only, for clarity. Black bars indicate the model predictions. (a) to (c): results for our azimuthal anisotropy model obtained from joint inversion of long period waveforms and station-averaged SKS data. (d) to (f): results from a model obtained using only surface waveforms. Predicted splitting is shown for integration of the models over, (a) and (d): the full depth range of the azimuthal anisotropy models, (b) and (e): the top 150 km of the models, (c) and (f): the portion of the model between 150 and 500 km, respectively.

model is 47%. Integrated over the full upper mantle depth range, our model predicts the circular pattern from the surface SKS measurements quite well (Fig. 7a) with a 58% variance reduction. We conclude that the circular pattern results from the combined effects of strong plate shear and varying depth dependent asthenospheric anisotropy in the western US, and their interaction with the craton boundary. Note that the smallest splitting times predicted by our model are in the central and southwest part of the Basin and Range province, consistent with the SKS splitting observations (Eakin et al., 2010; Liu, 2009; West et al., 2009).

Another important feature of the SKS measurements in the northwestern US region is the large measured splitting times. Xue and Allen (2006) observe a rotation of the splitting directions along a linear array from NW–SE in northwestern Oregon to East–West in southeastern Oregon, with an average of 1.65 s splitting time. From much denser 2D array stations, Long et al. (2009) see a similar change of splitting directions from central to eastern Oregon and western Idaho. Their measurements give an average of 2.0 s splitting time for the stations in the High Lava Plains. Strong mantle flow in the asthenosphere, presence of hydrous rocks in the upper mantle (Karato et al., 2008), and shape preferred orientation of partial melt, have been proposed to explain the anomalously large splitting times (Long et al., 2009). Our azimuthal anisotropy model predicts large splitting times and changes of the splitting directions in this region consistent with these previous studies (Fig. 7a). Interestingly Figure 7b indicates that the NE–SW North American APM parallel splitting direction originates most likely in the shallow portion of the upper mantle, due to the coupling between the upper plates (NA and Juan de Fuca, respectively) and the underlying shallow asthenosphere. Beneath Oregon and west Idaho in Figure 7c, significant East–West directed anisotropy, possibly representing a combined effect of: 1) edge flow along the craton southwestern margin at ~150 km depth; 2) the return flow due to the slab rollback at shallow depth; and 3) anisotropy fabrics in the stacked subducted slab segments (e.g., Schmid et al., 2002), contributes coherently to the East–West direction in the SKS splitting. The combination of both shallow and deep anisotropy thus can explain the large splitting times.

5. Comparison with MR07 model

Our new azimuthal anisotropy model of the western US shows large scale features that are generally consistent with those of our previous study (e.g. Fig. 1a–c in MR07). Some shorter wavelength features are present. In particular, below 100 km, the new model shows a significant transition from directions associated with plate motions at shallow depth to north and NNW fast axis direction in the southwestern US. East–West fast axis direction is found at 150 km under most of the Basin and Range and below 250 beneath the High Lava Plains. The new features are robust and a consequence of the significantly larger dataset available in the present study, allowing improved resolution.

Indeed, MR07 was obtained before the TA deployment. A total number of 45,000 surface waveform packets and a compilation of ~400 station-averaged SKS measurements were used in the inversion. The model was parameterized laterally in "level 4" spherical splines (8° spacing; corresponding to a degree 24 spherical harmonics model), and vertically in irregularly spaced 16 cubic splines (Fig. 3). The depth spline spacing in depth above the transition zone is ~100–150 km. As shown in Section 2, in the current inversion we are able to triple the amount of waveform and SKS data, and thus reach higher resolution both laterally and vertically (now at ~450 km spacing of spherical splines, corresponding to a degree 48 spherical harmonics model, and 30–70 km spacing of vertical splines; see Fig. 3). The increased lateral and vertical resolution has allowed shorter wave length features in our azimuthal anisotropy model, especially in the most data-rich western US region. Close inspection shows that, the

largest difference between the two models occurs in the Colorado Plateau and the southern Basin and Range, i.e. regions transitioning from the active western US region into the stable craton. While in model MR07, the signature of the craton spills over to the Colorado Plateau due to the long wavelength spherical splines used in that inversion, the smoothing effect is reduced in our higher resolution new inversion. Our resolution tests in Figure 4 and Supp. Figure 6–10 in (Yuan and Romanowicz, 2010) show that our current model resolves structures with ~450 km lateral wavelength and fast axis direction changes within ~30–40 km in depth. Thus we conclude these structural differences with MR07 are robust, and are attributed to the finer spatial resolution enabled by the new dataset.

The robustness of newly added features is also supported by higher variance reduction of the SKS data using our new model. The circular pattern in the SKS splitting measurements is well predicted by the new model (Fig. 7), which can explain 58% variance of the newly compiled SKS dataset, while the MR07 model can only explain 41% of these data. We do not expect to explain much more of the variance in the splitting data, because our model parameterization is still smooth compared to the sampling provided by the dense USArray deployment. Accordingly, Figure 7a shows our model does not predict the large apparent splitting times along the western boundary of the Colorado Plateau, the Sevier thrust and fold belt in Utah (Fig. 1), where very rapid lateral changes at (<100 km scale) in seismic velocities and shear wave splitting fast axis directions have been reported (Sine et al., 2008; Wang et al., 2008). This sharp boundary in seismic velocity and fast axis direction change is beyond our current resolution.

6. Discussion and conclusions

Results of synthetic tests presented in Figure 4 show that the depth dependence of azimuthal anisotropy described here is well resolved by the data and our inversion procedure. In particular, the joint inversion of waveform data and SKS splitting data is essential to recover the strength of azimuthal anisotropy at depths greater than 200 km and provides a more symmetric and uni-modal distribution of residuals in both fast axis direction and strength of anisotropy, than for the model based only on waveform inversion, as shown in Figure 8.

Since our long period waveform dataset does not have much sensitivity to crustal anisotropy, we do not invert for anisotropy at depths shallower than 24 km (the Moho depth in our reference 1D model), and only consider azimuthal anisotropy in the upper mantle. Shorter period azimuthal anisotropy studies (Beghein et al., 2010; Lin et al., 2009) reveal strong azimuthal anisotropy in the crust, likely reflecting strongly deformed crust and shallow upper mantle due to the Cenozoic Basin and Range extension (e.g., Jones et al., 1992; Moschetti et al., 2010). However, crustal thicknesses are smaller than 30 km in the region considered (e.g., Miller and Levander, 2009), and therefore cannot contribute more than ~0.2–0.3 s to SKS splitting times and cannot significantly affect the upper mantle structure found here, although they likely contribute to the remaining unexplained variance in both SKS splitting data and waveform fits.

Several azimuthal anisotropy studies using Rayleigh wave data have documented frequency dependent anisotropy in the western U.S. upper mantle, indicative of strong depth dependence. These studies use only the fundamental Rayleigh waves which have sensitivity from the crust down to ~200 km, and most of them only show phase velocity maps at different periods, stopping short of inverting with depth (e.g., Beghein et al., 2010; Li et al., 2005; Yang and Forsyth, 2006; Zhang et al., 2009). Our results in different parts of the western US are generally consistent with these studies. Some differences are found in the details. For example, west of the RMF, in the Colorado Rocky Mountains, Li et al. (2005) observe a significant trend of increasing anisotropy strength with period and suggest that the anisotropy domain beneath the Colorado Rockies is dominated by a source deeper than 100 km depth,
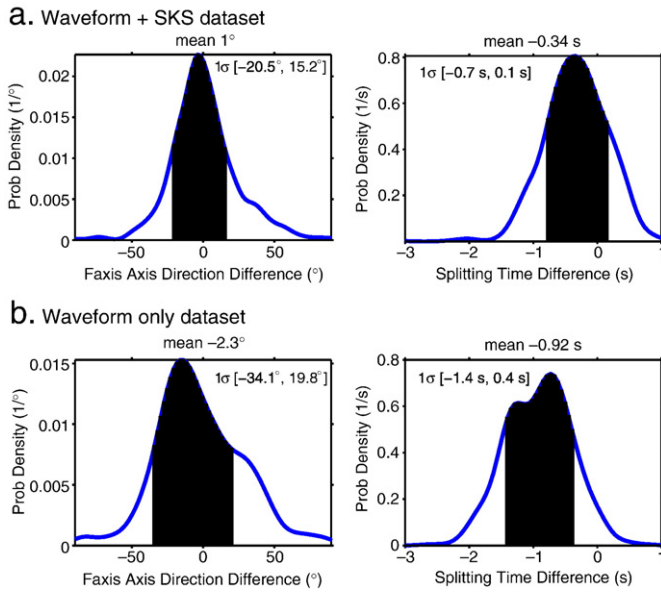
Fig. 8. Comparison of SKS misfits between the observations and predictions from the model obtained using: (a) waveforms and SKS data, jointly; (b) waveforms only. *Left panels*: probability density estimates for the difference in fast axis direction; *Right panels*: same for the difference in splitting time. The 1-σ region is colored in black. Note that the misfits from the joint inversion of waveforms and SKS data are centered closer to zero, and have a more uni-modal shape and smaller 1-σ region than those obtained from the model based on waveforms only.

possibly a highly anisotropic asthenosphere strongly sheared by the NA. They also point out that their strong and consistent anisotropy at longer periods is in contradiction to the SKS splitting measurements in the northern Colorado Rockies, where many null measurements are observed (Savage et al., 1996). We also observe a sharp transition across the RMF and NA APM directed fast axis above 150 km depth (Figs. 5 and 6), consistent with their results. At larger depths (>200 km) however, our model shows a second anisotropy domain with North–South directed fast axis (Fig. 5). Due to this deeper layer with nearly orthogonal fast axis direction, the overall predicted SKS splitting times from our model are small in this region (Fig. 7a), consistent with the SKS splitting measurements.

The notable East–West anisotropy direction beneath Nevada and central California at 150 km to 200 km depth beneath Oregon and Washington is supported by geodynamic modeling, as mentioned earlier. Silver and Holt (2002) consider a density driven eastward flow due to the sinking of the Farallon slab on the eastern border of the region. Becker et al. (2006) predict a similar East–West anisotropy direction above 200 km in this region, and their model suggests it is due to the complications of the flow field by the subducted Juan de Fuca slab (e.g., slab rollback). Alternatively, from a plate motion reconstruction, Zandt and Humphreys (2008) show the southern end of the slab window may extend into central Nevada. As indicated by the combination of North–South fast axis direction, slow velocities and radial anisotropy with ξ<1 south of the triple junction, the deep-seated active upwelling flow from the subducted East Pacific Rise, therefore, may be partially deflected to the east (Moucha et al., 2009) as it reaches the base of the Colorado Plateau in eastern Basin and Range.

Our upper mantle 3-D azimuthal anisotropy model shows strong lateral and vertical variations throughout the western US, which reflect complex past and present tectonic processes. To first order, the azimuthal anisotropy orientation reflects the gradual transition from a NA APM dominated pattern at shallow depths adjacent to the craton, to a Pacific Plate APM dominated pattern at greater depths on the ocean side. Our model successfully predicts the circular pattern of the SKS splitting measurements in the western US, which results from the depth-integrated effects of the lithosphere–asthenosphere coupling to the NA, Pacific and JdF plates at shallow depths, and in the depth range of 200–400 km, northward flow from the EPR channeled along the craton edge and deflected by the JdF slab, and more generally slab related anisotropy. With the accumulating high quality TA data, surface wave azimuthal anisotropy combined with multiple layer SKS splitting modeling (e.g., Levin et al., 1999; Özalaybey and Savage, 1994; Silver and Savage, 1994; Yuan et al., 2008) now make it possible to resolve complex depth dependent anisotropic domains in the North American upper mantle.

Acknowledgements

References

Abt, D., Fischer, K.M., French, S.W., Ford, H.A., Yuan, H.Y., Romanowicz, B., 2010. North American lithospheric discontinuity structure imaged by Ps and Sp receiver functions. J. Geophys. Res. 115 (B9), B09301. doi:10.1029/2009JB006710.

Bassin, C., Laske, G., Masters, G., 2000. The current limits of resolution for surface wave tomography in North America. Eos Trans. AGU 81, F897.

Becker, T.W., Schulte-Pelkum, V., Blackman, D.K., Kellogg, J.B., O'Connell, R.J., 2006. Mantle flow under the western United States from shear wave splitting. Earth Planet. Sci. Lett. 247, 235–251.

Beghein, C., Snoke, J.A., Fouch, M.J., 2010. Depth constraints on azimuthal anisotropy in the Great Basin from Rayleigh-wave phase velocity maps. Earth Planet. Sci. Lett. 289, 467–478.

Burchfiel, B.C., Cowan, D.S., Davis, G.A., 1992. Tectonic overview of the Cordilleran Orogen in the Western United States. In: Burchfiel, B.C., Lipman, P.W., Zoback, M.L. (Eds.), The Cordilleran Orogen; Conterminous U.S. The Geology of North America, v. G-3. Geol. Soc. Am, United States, Boulder, Colorado, pp. 407–479.

Burdick, S., van der Hilst, R.D., Vernon, F.L., Martynov, V., Cox, T., Eakins, J., Mulder, T., Astiz, L., Pavlis, G.L., 2009. Model update december 2008: upper mantle heterogeneity beneath North America from P-wave travel time tomography with global and USArray transportable array data. Seismol. Res. Lett. 80, 638–645.

Courtier, A.M., Gaherty, J.B., Revenaugh, J., Bostock, M.G., Garnero, E.J., 2010. Seismic anisotropy associated with continental lithosphere accretion beneath the CANOE array, northwestern Canada. Geology 38, 887–890.

Currie, C., Cassidy, J.F., Hyndman, R.D., Bostock, M.G., 2004. Shear wave anisotropy beneath the Cascadia subduction zone and western North American craton. Geophys. J. Int. 157, 341–353.

Davis, P.M., 2003. Azimuthal variation in seismic anisotropy of the southern California uppermost mantle. J. Geophys. Res. 109. doi:10.1029/2001JB000637.

Eakin, C.M., Obrebski, M., Allen, R.M., Boyarko, D.C., Brudzinski, M.R., Porritt, R., 2010. Seismic anisotropy beneath Cascadia and the Mendocino triple junction: interaction of the subducting slab with mantle flow. Earth Planet. Sci. Lett. 297, 627–632.

Favier, N., Chevrot, S., 2003. Sensitivity kernels for shear wave splitting in transverse isotropic media. Geophys. J. Int. 153, 213–228.

Forte, A.M., Moucha, R., Simmons, N.A., Grand, S.P., Mitrovica, J.X., 2010. Deep-mantle contributions to the surface dynamics of the North American continent. Tectonophysics 481, 3–15.

Fouch, M.J., Rondenay, S., 2006. Seismic anisotropy beneath stable continental interiors. Phys. Earth Planet. Inter. 158, 292–320.

Fouch, M.J., Fischer, K.M., Parmentier, E.M., Wysession, M.E., Clarke, T.J., 2000. Shear wave splitting, continental keels, and patterns of mantle flow. J. Geophys. Res. 105, 6255–6275.

Fox, O., Sheehan, A.F., 2005. Shear wave splitting beneath the CDROM transects. In: Randy, G., Karlstrom, K.E. (Eds.), The Rocky Mountain region—An Evolving Lithosphere: Tectonics, Geochemistry, and Geophysics, Geophysical Monograph, 154. American Geophysical Union, Washington DC.

Frederiksen, A.W., Ferguson, I.J., Eaton, D., Miong, S.K., Gowan, E., 2006. Mantle fabric at multiple scales across an Archean–Proterozoic boundary, Grenville Front, Canada. Phys. Earth Planet. Inter. 158, 240–263.

Gok, R., Ni, J.F., West, M., Sandvol, E., Wilson, D., Aster, R., Baldridge, W.S., Grand, S., Gao, W., Tilmann, F., Semken, S., 2003. Shear wave splitting and mantle flow beneath LA RISTRA. Geophys. Res. Lett. 30, 1614 doi:1610.1029/2002GL016616.

Gripp, A.E., Gordon, R.G., 2002. Young tracks of hotspots and current plate velocities. Geophys. J. Int. 150, 321–361.

Hartog, R., Schwartz, S.Y., 2000. Subduction-induced strain in the upper mantle east of the Mendocino triple junction, California. J. Geophys. Res. 105, 7909–7930.

Jones, C.H., Wernicke, B.P., Farmer, G.L., Walker, J.D., Coleman, D.S., McKenna, L.W., Perry, F.V., 1992. Variations across and along a major continental rift: an interdisciplinary study of the Basin and Range Province, western USA. Tectonophysics 213, 57–96.

Karato, S.-i., Jung, H., Katayama, I., Skemer, P., 2008. Geodynamic significance of seismic anisotropy of the upper mantle: new insights from laboratory studies. Annu. Rev. Earth Planet. Sci. 36, 59–95.

Kustowski, B., Ekstrom, G., Dziewonski, A.M., 2008. Anisotropic shear-wave velocity structure of the Earth's mantle: a global model. J. Geophys. Res. 113. doi:10.1029/2007JB005169.

Lekic, V., Romanowicz, B., 2010. A simple method for improving crustal corrections in waveform tomography. Geophys. J. Int. 182, 265–278.

Levin, V., Menke, W., Park, J., 1999. Shear wave splitting in the Appalachians and the Urals; a case for multilayered anisotropy. J. Geophys. Res. 104, 17,975–17,994.

Li, X.-D., Romanowicz, B., 1995. Comparison of global waveform inversions with and without considering cross-branch modal coupling. Geophys. J. Int. 121, 695–709.

Li, A., Forsyth, D., Fisher, K., 2005. Rayleigh wave constraints on shear-wave structure and azimuthal anisotropy beneath the Colorado Rocky Mountains. In: K.K., Keller, R. (Eds.), The Rocky Mountain Region—An Evolving Lithosphere: Tectonics, Geochemistry, and Geophysics, AGU Monograph, 154. American Geophysical Union, Washington DC.

Li, X., Yuan, X., Kind, R., 2007. The lithosphere–asthenosphere boundary beneath the western United States. Geophys. J. Int. 170, 700–710.

Lin, F.C., Ritzwoller, M.H., Yang, Y., Fouch, M.J., 2009. The stratification of azimuthal anisotropy in the western US. Eos Trans. AGU 90 (52) Fall Meet. Suppl., Abstracts DI52A-07.

Liu, K.H., 2009. NA-SWS-1.1: a uniform database of teleseismic shear wave splitting measurements for North America. Geochem. Geophys. Geosyst. 10. doi:10.1029/2009GC002440.

Liu, H., Davis, P.M., Gao, S., 1994. SKS splitting beneath southern California. Geophys. Res. Lett. 22, 767–770.

Long, M.D., 2009. Complex anisotropy in D″ beneath the eastern Pacific from SKS–SKKS splitting discrepancies. Earth Planet. Sci. Lett. 283, 181–189.

Long, M.D., Silver, P., 2009. Shear wave splitting and mantle anisotropy: measurements, interpretations, and new directions. Surv. Geophys. 30, 407–461.

Long, M.D., Gao, H., Klaus, A., Wagner, L.S., Fouch, M.J., James, D.E., Humphreys, E., 2009. Shear wave splitting and the pattern of mantle flow beneath eastern Oregon. Earth Planet. Sci. Lett. 288, 359–369.

Love, A., 1927. A Treatise on the Mathematical Theory of Elasticity. Cambridge University Press, Cambridge.

Maggi, A., Debayle, E., Priestley, K., Barruol, G., 2006. Azimuthal anisotropy of the Pacific region. Earth Planet. Sci. Lett. 250, 53–71.

Marone, F., Romanowicz, B., 2007. The depth distribution of azimuthal anisotropy in the continental upper mantle. Nature 447, 198–201.

Marone, F., Gung, Y., Romanowicz, B., 2007. Three-dimensional radial anisotropic structure of the North American upper mantle from inversion of surface waveform data. Geophys. J. Int. 171, 206–222.

McCrory, P., Blair, J.L., Oppenheimer, D.H., Walter, S.R., 2006. Depth to the Juan De Fuca slab beneath the Cascadia subduction margin—a 3-D model for sorting earthquakes. U.S. Geological Survey, Data Series 91, Version 1.2.

Mégnin, C., Romanowicz, B., 2000. The three-dimensional shear velocity structure of the mantle from the inversion of body, surface and higher-mode waveforms. Geophys. J. Int. 143, 709–728.

Menke, W., 1989. Geophysical Data Analysis: Discrete Inverse Theory (revised Edition). Academic, San Diego.

Miller, M.S., Levander, A., 2009. Lithospheric structure beneath the Colorado Plateau determined by receiver functions. American Geophysical Union, Fall Meeting 2009, abstract #U51D-07.

Montagner, J.P., 2002. Upper mantle low anisotropy channels below the Pacific Plate. Earth Planet. Sci. Lett. 202, 263–274.

Montagner, J.-P., Nataf, H.-C., 1986. A simple method for inverting the azimuthal anisotropy of surface waves. J. Geophys. Res. 91, 511–520.

Montagner, J.-P., Griot-Pommera, D.-A., Lave, J., 2000. How to relate body wave and surface wave anisotropy? J. Geophys. Res. 105, 19,915–19,027.

Moschetti, M.P., Ritzwoller, M.H., Lin, F., Yang, Y., 2010. Seismic evidence for widespread western-US deep-crustal deformation caused by extension. Nature 464, 885–889.

Moucha, R., Forte, A.M., Rowley, D.B., Mitrovica, J.X., Simmons, N.A., Grand, S.P., 2009. Deep mantle forces and the uplift of the Colorado Plateau. Geophys. Res. Lett. 36.

Nettles, M., Dziewoński, A.M., 2008. Radially anisotropic shear velocity structure of the upper mantle globally and beneath North America. J. Geophys. Res. 113. doi:10.1029/2006JB004819.

Özalaybey, S., Savage, M.K., 1994. Double-layer anisotropy resolved from S phases. Geophys. J. Int. 117, 653–664.

Özalaybey, S., Savage, M.K., 1995. Shear-wave splitting beneath western United States in relation to plate tectonics. J. Geophys. Res. 100, 18,135–18,149.

Panning, M., Romanowicz, B., 2006. A three-dimensional radially anisotropic model of shear velocity in the whole mantle. Geophys. J. Int. 167, 361–379.

Polet, J., Kanamori, H., 2002. Anisotropy beneath California; shear wave splitting measurements using a dense broadband array. Geophys. J. Int. 149, 313–317.

Rümpker, G., Tommasi, A., Kendall, J.M., 1999. Numerical simulations of depth-dependent anisotropy and frequency-dependent wave propagation effects. J. Geophys. Res. 104, 23141–23153.

Russo, R.M., 2009. Subducted oceanic asthenosphere and upper mantle flow beneath the Juan de Fuca slab. Lithosphere 1, 195–205.

Savage, M.K., 1999. Seismic anisotropy and mantle deformation; what have we learned from shear wave splitting? Rev. Geophys. 37, 65–106.

Savage, M.K., 2002. Seismic anisotropy and mantle deformation in the Western United States and Southwestern Canada. Int. Geol. Rev. 44, 913–937.

Savage, M.K., Sheehan, A.F., 2000. Seismic anisotropy and mantle flow from the Great Basin to the Great Plains, western United States. J. Geophys. Res. 105, 13,715–13,734.

Savage, M.K., Sheehan, A.F., Lerner-Lam, A., 1996. Shear wave splitting across the Rocky Mountain Front. Geophys. Res. Lett. 23, 2267–2270.

Schmid, C., Goes, S., van der Lee, S., Giardini, D., 2002. Fate of the Cenozoic Farallon slab from a comparison of kinematic thermal modeling with tomographic images. Earth Planet. Sci. Lett. 204, 17–32.

Schutt, D.L., Humphreys, E.D., 2001. Evidence for a deep asthenosphere beneath North America from western United States SKS splits. Geology 29, 291–294.

Schutt, D., Humphreys, E.D., Dueker, K., 1998. Anisotropy of the Yellowstone Hot Spot wake, eastern Snake River plain, Idaho. In: Plomerova, J., Liebermann, R.C., Babuska, V. (Eds.), Geodynamics of Lithosphere and Earth's Mantle; Seismic Anisotropy as a Record of the Past and Present Dynamic Processes. : Pure Appl. Geophys., 151. Birkhaeuser Verlag, Basel, Switzerland, pp. 443–462. 2–4.

Sieminski, A., Paulssen, H., Trampert, J., Tromp, J., 2008. Finite-frequency SKS splitting: measurement and sensitivity kernels. Bull. Seismol. Soc. Am. 98, 1797–1810.

Sigloch, K., McQuarrie, N., Nolet, G., 2008. Two-stage subduction history under North America inferred from multiple-frequency tomography. Nat. Geosci. 1, 458–462.

Silver, P.G., 1996. Seismic anisotropy beneath the continents; probing the depths of geology. Annu. Rev. Earth Planet. Sci. 24, 385–432.

Silver, P.G., Chan, W.W., 1991. Shear wave splitting and subcontinental mantle deformation. J. Geophys. Res. 96, 16,429–16,494.

Silver, P.G., Holt, W.E., 2002. The mantle flow field beneath western North America. Science 295, 1054–1058.

Silver, P.G., Savage, M.K., 1994. The interpretation of shear-wave splitting parameters in the presence of two anisotropic layers. Geophys. J. Int. 119, 949–963.

Sine, C.R., Wilson, D., Gao, W., Grand, S.P., Aster, R., Ni, J., Baldridge, W.S., 2008. Mantle structure beneath the western edge of the Colorado Plateau. Geophys. Res. Lett. 35.

Smith, D., Ritzwoller, M.H., Shapiro, N., 2004. Stratification of anisotropy in the Pacific upper mantle. J. Geophys. Res. 109. doi:10.1029/2004JB003200.

van der Lee, S., Nolet, G., 1997. Upper mantle S velocity structure of North America. J. Geophys. Res. 102, 22815–22838.

Vinnik, L.P., Farra, V., Romanowicz, B., 1989. Azimuthal anisotropy in the Earth from observations of SKS at GEOSCOPE and NARS broadband stations. Bull. Seismol. Soc. Am. 79, 1542–1558.

Waite, G., Schutt, D., L, R, Smith, B., 2005. Models of lithosphere and asthenosphere anisotropic structure of the Yellowstone hotspot from shear wave splitting. J. Geophys. Res. 110. doi:10.1029/2004JB003501.

Walker, K.T., Bokelmann, G.H.R., Klemperer, S.L., 2004. Shear-wave splitting beneath the Snake River Plain suggests a mantle upwelling beneath eastern Nevada, USA. Earth Planet. Sci. Lett. 222, 529–542.

Wang, Z., Dahlen, F.A., 1995. Spherical-spline parameterization of three-dimensional earth models. Geophys. Res. Lett. 22, 3099–3102.

Wang, X., Ni, J.F., Aster, R., Sandvol, E., Wilson, D., Sine, C., Grand, S.P., Baldridge, W.S., 2008. Shear-wave splitting and mantle flow beneath the Colorado Plateau and its boundary with the Great Basin. Bull. Seismol. Soc. Am. 98, 2526–2532.

West, J.D., Fouch, M.J., Roth, J.B., Elkins-Tanton, L.T., 2009. Vertical mantle flow associated with a lithospheric drip beneath the Great Basin. Nat. Geosci. 2, 439–444.

Wolfe, C.J., Silver, P.G., 1998. Seismic anisotropy of oceanic upper mantle; shear wave splitting methodologies and observations. J. Geophys. Res. 103, 749–771.

Wüstefeld, A., Bokelmann, G., Barruol, G., Montagner, J.-P., 2009. Identifying global seismic anisotropy patterns by correlating shear-wave splitting and surface-wave data. Phys. Earth Planet. Inter. 176, 198–212.

Xue, M., Allen, R.M., 2006. Origin of the Newberry Hotspot Track: evidence from shear-wave splitting. Earth Planet. Sci. Lett. 244, 315–322.

Xue, M., Allen, R.M., 2007. The fate of the Juan de Fuca plate: implications for a Yellowstone plume head. Earth Planet. Sci. Lett. 264, 266–276.

Xue, M., Allen, R.M., 2010. Mantle structure beneath the Western US and its implications for convection processes. J. Geophys. Res. 115, B07303. doi:10.1029/2008JB006079.

Yang, Y., Forsyth, D.W., 2006. Rayleigh wave phase velocities, small-scale convection, and azimuthal anisotropy beneath southern California. J. Geophys. Res. 111, B07306 07310.01029/02005jb004180.

Yuan, H., Romanowicz, B., 2010. Lithospheric layering in the North American Craton. Nature 466 (7310), 1063–1068.

Yuan, H., Dueker, K., Schutt, D., 2008. Testing five of the simplest upper mantle anisotropic velocity parameterizations using teleseismic S and SKS data from the Billings, Montana PASSCAL array. J. Geophys. Res. 113. doi:10.1029/2007JB005092.

Zandt, G., Humphreys, E., 2008. Toroidal mantle flow through the western US slab window. Geology 36, 295–298.

Zhang, X., Paulssen, H., Lebedev, S., Meier, T., 2009. 3D shear velocity structure beneath the Gulf of California from Rayleigh wave dispersion. Earth Planet. Sci. Lett. 279, 255–262.